Daclatasvir Prevents Hepatitis C Virus by Blocking Transfer of Viral Genome to Assembly Sites.

Bertrand Boson, Solène Denolly, Fanny Turlure, Christophe Chamot, Marlène Dreux, Cosset François-Loïc

Accepted Manuscript

Daclatasvir Prevents Hepatitis C Virus by Blocking Transfer of Viral Genome to Assembly Sites

Bertrand Boson, Solène Denolly, Fanny Turlure, Christophe Chamot, Marlène Dreux, François-Loïc Cosset

PII: S0016-5085(16)35447-6
DOI: 10.1053/j.gastro.2016.11.047
Reference: YGAST 60859

To appear in: *Gastroenterology*
Accepted Date: 28 November 2016

Please cite this article as: Boson B, Denolly S, Turlure F, Chamot C, Dreux M, Cosset F-L, Daclatasvir Prevents Hepatitis C Virus by Blocking Transfer of Viral Genome to Assembly Sites, *Gastroenterology* (2017), doi: 10.1053/j.gastro.2016.11.047.

Daclatasvir Prevents Hepatitis C Virus by Blocking Transfer of Viral Genome to Assembly Sites

Short title: DCV impairs HCV RNA transfer to assembly site

Authors: Bertrand Boson[1], Solène Denolly[1], Fanny Turlure[1], Christophe Chamot[2], Marlène Dreux[1,*], François-Loïc Cosset[1,*]

[1]CIRI – International Center for Infectiology Research, Team EVIR, Inserm, U1111, Université Claude Bernard Lyon 1, CNRS, UMR5308, Ecole Normale Supérieure de Lyon, Univ Lyon, F-69007, Lyon, France.
[2]PLATIM, US8 / UMS3444 BioSciences Gerland, Lyon, France.
*These authors contributed equally to the work

Grant support: This work was supported by the French “Agence Nationale de la Recherche sur le SIDA et les hépatites virales” (ANRS), the European Research Council (ERC-2008-AdG-233130-HEPCENT) and the LabEx Ecofect (ANR-11-LABX-0048).

Abbreviations: HCV, hepatitis C virus; DCV, Daclatasvir; RNA, ribonucleic acid; RC, replication complex; DAA, direct-acting antiviral; NS, nonstructural protein; EC, effective concentration; DMV, double membrane vesicle; FFU, focus-forming unit; MOI, multiplicity of infection; CHX, cycloheximide; ER, endoplasmic reticulum; LD, lipid droplet; SIM, Structured Illumination Microscopy; DGAT1, diacylglycerol acyltransferase-1; FISH, Fluorescent *In-Situ* Hybridization; GE, genome equivalent; ns, not significant; ND, not determined; CTD, C-terminal domain.

Correspondence: François-Loïc Cosset. CIRI – International Center for Infectiology Research, Université de Lyon, Lyon, France. E-mail: flcosset@ens-lyon.fr

Disclosures: the authors disclose no conflicts.

Author contributions: Study concept and design: BB, FLC. Acquisition of data: BB, SD. Analysis and interpretation of data: BB, SD, FT, CC, MD, FLC. Drafting of the manuscript: BB, SD, MD, FLC. Material support: CC.

Acknowledgments

We are grateful to Ralf Bartenschlager for the gift of JFH1, Jc1 and Jc1-Y93H constructs, Charles Rice for the gift of Huh7.5 cells and 9E10 monoclonal NS5A antibody, Mishinori Kohara for the gift of NS4B antibody, Jane McKeating for the gift of 3/11 E2 antibody and Colette Jolivet for the gift of core antibody. We thank François Penin for helpful comments and critical reading of the manuscript. We thank Claire Lionnet and Elodie Chatre for excellent technical assistance with confocal microscopy.

We dedicate this paper to the memory of our colleague and friend Pr. Christophe Terzian.

Abstract:

BACKGROUND & AIMS: Daclatasvir is a direct-acting antiviral agent and potent inhibitor of NS5A, which is involved in replication of the hepatitis C virus (HCV) genome, presumably via membranous web shaping, and assembly of new virions, likely via transfer of the HCV RNA genome to viral particle assembly sites. Daclatasvir inhibits the formation of new membranous web structures and, ultimately, of replication complex vesicles, but also inhibits an early assembly step. We investigated the relationship between daclatasvir-induced clustering of HCV proteins, intracellular localization of viral RNAs and inhibition of viral particle assembly.

METHODS: HCVcc particles were produced from Huh7.5 hepatocarcinoma cells in presence of daclatasvir for short time periods. Infectivity as well as production of physical particles were quantified and producer cells were subjected to subcellular fractionation. Intracellular colocalization between core, E2, NS5A, NS4B proteins, and viral RNAs was quantitatively analyzed by confocal microscopy and by structured illumination microscopy.

RESULTS: Short exposure of HCV-infected cells to daclatasvir reduced viral assembly and induced clustering of structural proteins with non-structural HCV proteins, including core, E2, NS4B and NS5A. These clustered structures appeared to be inactive assembly platforms, likely owing to loss of functional connection with replication complexes. Daclatasvir greatly reduced delivery of viral genomes to these core clusters without altering HCV RNA colocalization with NS5A. In contrast, daclatasvir neither induced clustered structures nor inhibited HCV assembly in cells infected with a daclatasvir-resistant mutant (NS5A-Y93H), indicating that daclatasvir targets a mutual, specific function of NS5A inhibiting both processes.

CONCLUSIONS: In addition to inhibiting replication complex biogenesis, daclatasvir prevents viral assembly by blocking transfer of the viral genome to assembly sites. This leads to clustering of HCV proteins, because viral particles and replication complex vesicles cannot form and/or egress. This dual mode of action of daclatasvir could explain its efficacy in blocking HCV replication in cultured cells and in treatment of patients with HCV infection.

KEY WORDS: chronic hepatitis C; direct-acting antiviral agent; DAA

Introduction

Hepatitis C virus (HCV) infection is a leading cause of chronic liver diseases world-wide. With 180 million people persistently infected, chronic HCV infection, which induces end-stage liver diseases such as liver cirrhosis and hepatocellular carcinoma, presents a public health problem of high socio-economic impact. No protective vaccine exists against HCV. However, the development of direct-acting antivirals (DAAs) targeting different proteins and functions in HCV life cycle has dramatically changed the treatment options for chronic hepatitis C, leading to new hopes to cure HCV from infected patients.

HCV has a positive-sense single-strand RNA (RNA(+)) genome encoding viral proteins including: i) an assembly module (C–NS2) encompassing the capsid protein (core) as well as the E1 and E2 surface glycoproteins that are incorporated in viral particles, and the p7 viroporin and NS2 protein that support virion assembly, and ii) a replication module encompassing the nonstructural (NS) proteins NS3, NS4A, NS4B, NS5A and NS5B that are sufficient to support viral RNA replication and that also contribute to virion formation through an unclear process.

The recent development of DAAs has greatly benefited from discoveries in HCV molecular virology and host/virus interactions[1]. The primary targets of DAAs include[2] the serine protease activity of NS3/NS4A, the multifunctional RNA-binding phosphoprotein NS5A and the RNA-dependent RNA polymerase NS5B. Daclatasvir (DCV) and DCV-related molecules were discovered through screening of compounds inhibiting HCV subgenomic replicons[3]. In addition to being effective inhibitors of HCV replication, with EC_{50} values in the pM range, recent studies have reported that DCV acts on a distinct stage of replication (viral particle assembly)[4-6]. Exposure of HCVcc-infected cells to DCV for short time periods decreased production of infectious particles before decay of intracellular HCV RNA and polyprotein levels.

Although DCV's mode of action is unclear, it specifically targets NS5A[3,7]—particularly its domain I (DI), which has functions associated with genome replication[8], in line with identified DCV-resistant mutations in DI (*e.g.*, L31 and Y93)[3]. Importantly, DCV inhibits formation of double-membrane vesicles (DMVs) that contain the HCV RNA replication complex (RC)[6,9] and are induced by non-structural proteins—particularly NS4B and NS5A[10,11]. Moreover, other studies reported that DCV or DCV-related compounds decrease mobility[12], intracellular redistribution[13,14] and/or clustering[5,12,15] of NS5A. Despite these remarkable findings, there is no clear consensus on the role, location, and kinetics of these events, possibly because of

differences in experimental conditions. NS5A is an HCV RNA-binding protein[16,17] that mediates HCV RNA transfer to viral particles[18], so it seems possible that altered NS5A intracellular localization and/or trafficking could prevent assembly of infectious particles.

We investigated the relationship between DCV-induced clustering of HCV proteins and inhibition of viral particle assembly. We studied the intracellular localization of HCV assembly and RC proteins along with HCV RNA(+) and RNA(-) species within HCV-infected cells at early time points following DCV exposure, and compared these events with the production of infectious particles. We show that in addition to inhibiting DMV biogenesis, DCV prevents HCV assembly by blocking the transfer of viral genomes to virion assembly proteins. This leads to clustering of HCV proteins, likely because viral particles and RC vesicles cannot form and/or egress from the endoplasmic reticulum (ER) membranes. This dual mode of action of DCV could account for its extremely high potency in cell culture and, most likely, in patients.

Materials and Methods

Cell culture and reagents. Huh7.5 cells were grown in Dulbecco's modified minimal essential medium (DMEM, Invitrogen, France) supplemented with 100U/ml of penicillin, 100µg/ml of streptomycin, and 10% fetal bovine serum.

Expression constructs. pFK-JFH1wt_dg, pFK-JFH1/J6/C-846_dg and pFK-Jc1-Y93H_dg plasmids[6,19] were kind gifts from R. Bartenschlager.

HCVcc production and titration. HCVcc production procedures were described previously[20]. Supernatants infectivity titers were determined as focus-forming units (FFU/ml). Serial dilutions of supernatants were used to infect Huh7.5 cells, FFUs were determined 3 days post-infection by counting NS5A-immunostained foci.

Immuno-fluorescence (IF) and confocal microscopy imaging. Huh7.5 cells grown on uncoated 14mm-diameter glass coverslips were infected at MOI of 0.2. At indicated times post-infection, cells were washed with PBS, fixed with 3% paraformaldehyde in PBS for 15min, quenched with 50mM NH_4Cl and permeabilized with 0.1% Triton X-100 for 7min. Fixed cells were then incubated for 1h with primary antibodies in 1% BSA/PBS, washed and stained for 1h with the corresponding fluorescent Alexa-conjugated secondary antibody (Alexa-488, Alexa-555 and Alexa-647, Molecular Probes Europe BV, The Netherlands) in 1%

BSA/PBS. LDs were stained with 10µg/mL Bodipy 493/503 (Molecular Probes) according to the manufacturer's instructions. Cells were washed three times with PBS, stained for nuclei with Hoechst (Molecular Probes) for 5min when stated, washed and mounted in Mowiol prior to image acquisition with LSM-510 or LSM-710 confocal microscopes.

Combined detection of HCV RNA by Fluorescent *In Situ* Hybridization (FISH) and viral proteins. Viral proteins were first immunostained as described above. After a post-fixation step with 3% paraformaldehyde for 15min and 3 washes with PBS, HCV RNA(+) and RNA(-) strands were detected using probe sets that target regions between nucleotide positions 3733-4870 and 4904–5911, respectively, in the JFH1 genome using QuantiGene ViewRNA ISH Cell Assay kit (Panomics/Affymetrix, USA) according to the manufacturer's instructions, except for the protease digestion step that was omitted. Omission of protease digestion step did not affect detection of HCV RNA(+) or RNA(-) foci (data not shown). Nuclei staining, slide mounting and acquisition were performed as above-described.

Structured Illumination Microscopy. Huh7.5 cells were grown on high precision cover glasses and infected (MOI=0.2). 72h post-infection, cells were fixed with 3% paraformaldehyde and stained as above-described. Cells were then mounted in Fluoromount-G prior to image acquisition with Elyra PS-1 microscope. Images were reconstructed using the Zen 2012 Black software.

Image analysis and quantifications. Images were analyzed with the ImageJ software. For quantifications of structures, colocalized pixels were extracted with the ColocalizeRGB plugin with auto-thresholding and a pixel ratio between paired channels set to 50%. They were then segmented with the Watershed algorithm and quantified with the Analyze Particles function of ImageJ. Only structures with size >0.02µm^2, which corresponds to half of the resolution limit of confocal laser scanning microscopy, were recorded. For quantification of structures apposed at the edge of LDs, an ImageJ macro was developed (for details, see Supplemental Results) to search for variation of max intensity in the neighborhood of each LD as an indicator of proximity. Structures distant from LDs by more than 3 pixels (ca. 205-207nm) were considered as non-apposed at the edge of LDs. When stated, the Pearson's correlation coefficients were calculated by using the JACoP plugin.

Statistical analysis. Significance values were calculated by applying the two-tailed, unpaired Mann-Whitney test for image analyses and the paired t-test for the quantification of viral RNA, core protein and infection assays, using the GraphPad Prism 6 software (GraphPad Software, USA). P values under 0.05 were considered statistically significant and

the following denotations were used: ****, P≤0.0001; ***, P≤0.001; **, P≤0.01; *, P≤0.05; ns (not significant), P>0.05.

Results

An NS5A inhibitor preventing viral assembly induces co-clustering of structural and non-structural proteins. To understand DCV impact on viral particle assembly, first, we confirmed and extended previous studies[4,5] indicating that, unlike the DCV-resistant NS5A-mutant Jc1-Y93H virus[6], a 6h-long treatment with 1nM DCV had no effect on intracellular HCV RNA (Supplemental Figure 1A, left panels) and core protein (right panel) levels in cells infected with Jc1 virus. In contrast, a longer treatment (24h) reduced Jc1 intracellular RNAs by over 10-fold, in accordance with these former reports. As reported previously[4,5], inhibition of infectivity was detectable from 2h after the initiation of DCV treatment (Supplemental Figure 2A-B). Upon a 6h-long treatment, the levels of both intra-cellular and extra-cellular infectious particles were reduced by *ca*. 13 and 4-fold, respectively, whereas Jc1-Y93H virus infectivity was not affected (Supplemental Figures 1B and 2A-B). Finally, we found that DCV inhibited the production of physical particles (Supplemental Figure 1C), as judged by the inhibition of both secreted viral RNAs and core protein from infected cells. Altogether, these results indicated that the decrease of viral production *via* short-time DCV treatment is due to inhibition of viral assembly rather than egress of particles, whereas longer treatments inhibit both assembly and replication.

Since DCV alters NS5A intracellular distribution[5,12-15] and since core colocalizes with several other HCV proteins in Jc1-infected cells, including E2, NS2, NS3, NS4B and NS5A (Supplemental Figure 3), we next wondered if DCV inhibits viral assembly by altering the association of structural proteins with non-structural proteins from RCs. Thus, we investigated by confocal microscopy the effect of short-time DCV treatments on HCV proteins that mark either component of viral particles[20], *i.e*., core and E2, or RCs[10,21], *i.e*., NS5A (Figure 1) and NS4B (Figure 2). Importantly, punctate structures colocalizing E2, core and NS5A proteins were readily detected in Jc1-infected cells at 72h post-infection (see the extractions of E2/core/NS5A colocalization pixels in the right panels A of either figure and quantifications in panels B-C). Strikingly, after a 6h-long DCV treatment, they appeared *ca*. 85% bigger than without treatment (Figure 1B). Likewise, E2/core/NS4B punctate structures were also detected in Jc1-infected cells (Figure 2); yet, similar to E2/core/NS5A structures, their size steadily increased from 2h after DCV treatment (Supplemental Figure 2C) and was *ca*. 75% bigger than without DCV treatment after a 6h-long incubation (Figure 2B), although

their number remained constant (Supplemental Figure 2D, Figure 2C). Of note, short-time DCV treatments from 18h post-infection also induced strong enlargements of both E2/core/NS5A and E2/core/NS4B punctate structures, by up to 3-fold (data not shown). These core/NS5A and core/NS4B structures clustering with E2 (Figures 1 and 2) likely gathered within combined structures, as indicated by the enlargement of punctae that included core, NS5A and NS4B upon short-time DCV treatments (Supplemental Figure 4). Importantly, the Y93H DCV-resistant mutation abolished DCV-induced enlargement of all these structures (Figures 1 and 2, Supplemental Figure 2C-D), indicating that their alteration likely involved DCV effect on NS5A.

Finally, DCV treatment blocked NS5A hyper-phosphorylation, as shown by others[22,23], which correlated with the co-clustering of structural and non-structural proteins and with the concomitant decrease of assembly of infectious viral particles (Supplemental Figures 5 and 2). As noted by others[6,22], the Y93H DCV-resistant mutation altered DCV-mediated inhibition of NS5A hyper-phosphorylation (Supplemental Figure 5). As NS5A hyper-phosphorylation modulates NS5A functions in both replication and assembly[8], these results further implied that DCV targeting of NS5A DI domain function(s) is pivotal for both steps.

Altogether, these results suggested that DCV acts shortly after administration to block viral assembly and results in the co-clustering of structural proteins with RC components.

In absence of DCV treatment, structural and non-structural proteins colocalize over-time post-infection within accruing punctate structures. Our results suggested that, rather than inducing novel structures, DCV expands and/or merges preexisting structures colocalizing structural and non-structural proteins. Accordingly, DCV did not modify the cellular localization and membrane association of E2, core, NS4B and NS5A proteins, as indicated by subcellular fractionation assays of infected cells that did not reveal changes in their fraction contents upon DCV treatment (Supplemental Figure 6A). Altogether, this prompted us to characterize such preexisting structures, aiming at understanding the mode of action of DCV on HCV assembly inhibition.

Using super-resolution microscopy (3D-SIM), we found that E2/core/NS4B dot structures gather NS4B part(s) and E2-dense parts, with core joining either areas (Figure 3A). Such structures might represent territories connecting the sites of replication and assembly. Hence, to investigate their formation, they were characterized over time post-infection with the Jc1 virus comparatively to the JFH1 virus that produces 50-100 fold less infectious viral particles[20] despite identical replication rates[19]. At early timepoints post-infection (before 24h), core and/or NS4B appeared as punctate structures whereas E2 was spread throughout the ER (Figure 4A, Supplemental Figure 7). Few dots of colocalization between core, E2 and NS4B were detected at early timepoints in both Jc1- and JFH1-infected cells; yet, their

number increased subsequently. Specifically, from 24h to 72h post-infection, the number and size of E2/core/NS4B structures increased in Jc1-infected cells by *ca*. 20- and 3-fold, respectively (Figure 4B-C). This suggested that core progressively concentrates in areas including E2 and/or NS4B, and that the structures containing both structural proteins and components of RCs appear concomitantly. Comparatively, the number and size of E2/core/NS4B structures increased slowly in JFH1 virus-infected cells from 24h post-infection and were *ca*. 10-fold less frequent at 72h post-infection as compared to Jc1 (Figure 4B), in agreement with the lower production of infectious viral particles (Figure 4D). Thus, the appearance of E2/core/NS4B structures, which correlated with infectivity levels, suggested that they could represent RCs connected to viral particle assembly components or sites.

DCV does not alter the localization of punctate structures that are apposed to, but not associated to LDs. Previous studies reported a differential accumulation of HCV core in two distinct intracellular areas in Jc1- *vs*. JFH1-infected cells, *i.e*., at the ER *vs*. LDs[20,24], respectively, which may reflect the dissimilar capacity of core from either virus to engage in assembly. Thus, aiming at better characterizing the initiation of HCV assembly, we compared core localization at different timepoints post-infection. At 16h post-infection, the core protein showed intracellular localization patterns as small and discrete punctae that were distributed uniformly (Supplemental Figure 8A). These structures were still observed at 24h post-infection for both viruses; yet, in JFH1-infected cells, core became also detectable at the surface of LDs. At later timepoints, from 48h post-infection, the core protein was found clearly redistributed following two different patterns, *i.e.* as a reticular pattern in Jc1-infected cells *vs*. surrounding LDs in JFH1-infected cells (Supplemental Figure 8A).

To determine how the initial core punctae were progressively redistributed in either pattern, we inhibited protein synthesis at 24h *vs*. at 48h post-infection by treating infected cells with cycloheximide (CHX) for 24h (Supplemental Figure 8A). Following CHX-treatment, the core protein of JFH1 virus was still observed as ring-like structures that completely surrounded over 95% of the LDs, suggesting that the core protein initially present as discrete punctae progressively reached and accumulated at LD surface. In sharp contrast, the early-detected discrete core punctae persisted in CHX-treated Jc1-infected cells and enlarged by *ca*. 50% from 48h to 72h post-infection (Supplemental Figure 8A-B).

When we determined the localization of these core punctae in Jc1-infected cells, we found that they were not randomly distributed throughout the ER but rather, that a significant part, of *ca*. 40%, was apposed at the edge of LDs (Figure 5A-B), which represent specific sites where LDs are juxtaposed to the ER membrane and may gain their proteins[25]. As about 10% of LDs in Jc1-infected cells were surrounded by core protein compared to over 95% in JFH1-infected cells (Figure 5C), this suggested that core-apposition at LD edges, rather than LD

surface-association, promotes HCV early assembly steps. These findings implied that the core protein of Jc1 virus was not mobilized to/from the LD surface, but rather, was targeted and/or retained at ER membrane sites apposed to LDs. This also indicated that the reticular pattern detected at late timepoints post-infection in CHX-untreated cells reflected the progressive accrual and/or enlargement of core punctae (Supplemental Figure 8A). Altogether, these results suggested that the association of core on LD surface does not contribute to virion assembly, at least in a direct manner, and that, over time post-infection, the core protein of the highly infectious Jc1 virus progressively concentrates in large, LD edge-apposed punctate structures, which is concomitant to virus production.

It is expected from the above findings that a part of the punctae in which core accumulated represented assembly sites. To characterize the connection of these dots with replication sites, we investigated the intracellular localization of core punctae colocalizing with the non-structural proteins revealed above, *i.e.*, NS5A and NS4B (Figures 1 and 2). Interestingly, both structures frequently localized (*ca*. 40-55%) at the edge of LDs in Jc1-infected cells (Figure 5D). By super-resolution microscopy, we found that core/NS4B dotted structures apposed at LD edges exhibited a bipolar arrangement, separating by *ca*. 0.1µm core on the one side and NS4B on the other side (Figure 3B). Importantly, a similarly high proportion of core/NS4B and core/NS5A structures remained apposed at the edges of LDs in infected cells treated or not with DCV (Supplemental Figure 6B), which further implied that DCV did not inhibit HCV assembly by altering localization of assembly proteins.

DCV prevents HCV genome transfer to virus-induced structures that may represent assembly platforms. At first sight, the increasing size of E2/core/NS4B structures during the infection course (Figure 4) seemingly contradicted the fact that DCV treatment could also induce their enlargement (Figure 2). As DCV inhibits viral particle assembly, we thought that this apparent paradox reflects the accumulation of proteins at assembly and RC sites. To test this hypothesis, we reasoned that impairing cellular assembly factors would similarly induce the expansion of E2/core/NS5A and/or E2/core/NS4B structures. Hence, we targeted DGAT1 (diacylglycerol acyltransferase-1), a factor that regulates HCV assembly by attracting core and NS5A proteins onto the surface of the same LDs[26,27]. Upon DGAT1 down-regulation or chemical inhibition, which reduced infectivity by *ca*. 9-fold, we found that both E2/core/NS5A and/or E2/core/NS4B structures enlarged, by up to 2-fold (Supplemental Figure 9). In a similar manner, we surmised that, owing to the dual role of NS5A in replication *vs*. packaging of HCV RNA[8,18], the enlargement of either structure upon short-time DCV treatment (Figures 1 and 2) may reflect a loss of functional transition from HCV replication to assembly as caused by defective NS5A-targeting of the viral genome to assembly components, ultimately resulting in their aggregation as inactive structures.

Thus, to further address this possibility, we thought to investigate whether the viral genome and its replicative intermediate, *i.e.,* HCV RNA(+) and RNA(-) species, respectively, could be found within these structures and could be altered upon DCV treatment. We therefore combined immunofluorescence analysis to label core, NS4B and NS5A proteins with fluorescence *in situ* hybridization (FISH) to detect HCV RNA(+) and RNA(-) strands, which appeared as dots that could represent sites of either translation, replication, viral assembly, or intracellular particles[28]. Importantly, both HCV RNA(+) and RNA(-) were detected within core/NS5A and core/NS4B structures, which further suggested that they represent, at least partly, assembly structures connected with RCs (Figure 6A, 6B-C: panels a-b). Interestingly, a 6h-long DCV-treatment did not change the proportion of either protein structure colocalizing with both types of RNAs (panels a-b). However, when we quantified the number of RNA dots colocalizing with HCV protein dots in Jc1-infected cells, we found that such DCV-treatment specifically decreased by up to 3-fold the proportion of HCV RNA(+) dots colocalizing with either core or NS4B punctae, whereas no changes were observed in Jc1-Y93H infected cells (panels c-d). In contrast, the proportion of HCV RNA(+) dots colocalizing with NS5A structures remained unchanged (panel e), implying that DCV-mediated NS5A inhibition acts downstream of NS5A/RNA interaction(s), in agreement with previous reports indicating that DCV does not inhibit HCV RNA binding to NS5A[14,29]. Finally, DCV did not change the proportion of HCV RNA(-) colocalizing with NS4B, NS5A and core in neither Jc1 nor Jc1-Y93H infected cells (Figure 6A, 6C). Altogether these observations suggested that DCV inhibited assembly by blocking the formation of active, i.e., RNA(+) containing, assembly sites.

Discussion

Our results uncover novel features of DCV-mediated HCV inhibition that further our understanding of HCV assembly. We confirmed that DCV induces NS5A clustering, in line with previous studies[5,12,15]. Interestingly, we found that other HCV proteins, such as E2, core and NS4B, gathered with these NS5A clusters (Figures 1 and 2, Supplemental Figure 4). We also found that the enlargement of these clusters upon short-time DCV treatments correlated with the reduction of viral particle assembly. As discussed below, we propose that DCV-induced accretion of HCV proteins reflects the loss of functional association between HCV replication and assembly.

Connection between RCs and assembly sites at LD proximity. Overall, our imaging, biochemical and functional data are congruent with a model previously proposed by others[21]

wherein assembly sites are closely associated to RCs and LDs in a micro-environment favoring replication, mobilization and protection of HCV RNA. First, by comparing the poorly infectious JFH1 virus *vs*. the highly infectious Jc1 virus, we found that the occurrence and intracellular localization of E2/core/NS4B and E2/core/NS5A structures were intimately related to infectivity levels (Figure 4) and that such structures were frequently apposed at the edge of LDs, *i.e.*, close to the ER membrane, but were not associated around or at LD surface (Figure 5). Second, through time-course analysis of infection combined with translation inhibition assays (Supplemental Figure 8), we highlighted the progressive accumulation of core punctae at ER membranes, which ultimately appeared as a mesh distributed throughout the ER, and their rapid and strong colocalization with HCV glycoproteins. Third, we found that a significant proportion (*ca*. 15-20%) of core/NS4B and core/NS5A structures contain HCV RNAs (Figure 6). Finally, our data underscored that the structures associating RNA(+), core and E2 structural components (*i.e.*, representing, at least in part, assembly sites[28]) with RCs and LDs[21], evolve in a very dynamic process both naturally and in response to specific inhibitors.

DCV induces clustering of viral proteins by altering both assembly and RC formation. We noticed that a high proportion (*ca*. 80-85%) of core/NS4B and core/NS5A structures do not contain HCV RNAs. We propose that such structures may represent assembly sites for which functional linkage with RCs or, alternatively, viral RNA transfer to nascent virions have waned or not occurred. Intuitively, one may expect that functional assembly sites would be difficult to seize, as they are necessarily transient, owing to release of assembled viral particles from such sites into the ER lumen and secretion by the cell. Moreover, that HCV RNA seems rate-limiting for inducing functional assembly is congruent with other findings that functional RCs, represented by DMVs having a cytosol-oriented orifice allowing release of newly synthesized HCV RNA, account for less than 10%[10], and that HCV RNA triggers viral particle envelopment[18]. Furthermore, HCV assembly is a poorly efficient process, in line with a general notion that the vast majority of structural proteins are not engaged or consummated in virions production. Accordingly, the progressive accumulation and enlargement of core-dotted structures appearing as a mesh in Jc1-infected cells (Supplemental Figure 8) likely revealed accretion of non-functional assembly sites or, corollary, of residual core proteins that have not engaged in assembled and/or released virions. In support of this view, we found that such core punctae do not arise from mobilization of LD-associated core but rather from their multiplication throughout the ER (Supplemental Figure 8), while replication and translation progresses, and from their enlargement following ER targeting.

In this respect, our unexpected finding that DCV accentuated the clustering and/or enlargement of core punctae concomitant to inhibition of assembly may likely reflect an accrued accumulation of non-functional assembly sites, *i.e*., of core proteins not recruited or released as infectious viral particles. Furthermore, we observed that both E2/core/NS4B and E2/core/NS5A structures also enlarged upon DCV treatment, concomitant to assembly inhibition. Finally, inhibiting assembly by targeting DGAT1, which promotes localization of core and NS5A at LDs[26,27], also resulted in enlargement of either structure (Supplemental Figure 9). However, these observations are not paradoxical if one considers that a majority of such structures are not functionally connected to on-going assembly events. Indeed, expression of HCV proteins continuously raises several vesicle types that are formed from the ER membrane, particularly viral particles and DMVs. Therefore, the release of the two latter vesicles, respectively within the ER lumen and the cytosol, as well as their turnover through secretion and/or degradation requires an unceasing creation of areas forming novel assembly sites and RCs. In this regard, NS5A, which intersects cellular degradation machineries, *e.g*., autophagy[30], might be pivotal for DMV turnover.

Importantly, since the Y93H mutation in NS5A renders both assembly and DMV biogenesis events resistant to DCV[6,9], it implies that DCV targets a mutual, specific NS5A function that inhibits both processes. Indeed, NS5A, in concert with CypA[9,31] and NS4B[10,11,32,33], has the capacity to induce DMV biogenesis through binding of its AH N-terminal amphipathic helix on the ER membrane and, as previously proposed[1,6,34-36], NS5A multimerization. Since DCV binds close to the amino-terminus of the DI domain of NS5A dimer, *i.e*., at the junction of both DI subunits and their interface with the ER membrane[1,6,7,35], DCV binding could perturb the positioning, orientation or flexibility of the AH helix that anchors NS5A. Thereby, this could alter the membranotropic properties of NS5A by altering its membrane binding, multimerization and/or interaction with partners, which would explain DCV capacity to inhibit the formation of DMVs[6,9] and subsequent RNA synthesis and/or trafficking[5] but also its lack of effect on replication within preexisting DMVs[9]. Owing to the fast turnover of DMVs[6], this inhibition would progressively lead to decay of HCV RNAs[5] by loss of newly formed DMVs. As a result, *de novo*-expressed non-structural proteins would tend to accumulate because their lack of segregation as DMVs would enhance the clustering of NS5A[5,12,15] and NS5B[12], as previously reported, but also of NS4B (this report) at ER membrane domains where DMVs form.

DCV prevents the delivery of viral genomes to assembly sites. It is unlikely that inhibition of DMV biogenesis explains the nearly immediate effect of DCV on assembly of infectious particles[4-6]. However, another important finding of our study was that short-time DCV treatments that prevented HCV assembly strongly reduced the colocalization of core with

HCV RNA(+) strand (Figure 6), which likely precluded formation of infectious particles (Supplemental Figure 1). Furthermore, since DCV had no effect on colocalization of viral RNA with core/NS4B and core/NS5A structures (Figure 6), we propose that, reminiscent of specific NS5A mutants in domain DIII that affect core/NS5A interaction[18], this could be due to a lack of transfer of viral genomic RNA to assembling virions. Indeed, DCV-mediated inhibition of DMV formation[6,9] may not result, *per se*, in the blockage of HCV RNA packaging or transfer since RNA synthesis may not occur before DMVs become fully formed and active[5]. Rather, we propose that DCV restrains preexisting, replication-active DMVs, *i.e*., among those already present at the onset of DCV treatment, from mediating this critical event in infectious particles assembly by targeting the same function of NS5A as above-described, *i.e*., its membranotropic properties. Indeed, transfer of HCV RNA from active DMVs to assembly sites would also be precluded if the membrane-binding properties of NS5A were altered for different, albeit not exclusive reasons. First, as NS5A is located both inside and outside DMVs[37], such alterations would compromise the stability of DMV surface-associated NS5A, and, consequently, the gathering of replication-active DMVs at the vicinity of HCV particle assembly sites and/or of LDs, because this targeting depends on core and NS5A interaction[21,38,39] and is critical for mediating RNA transfer to the core protein[18]. Second, as NS5A is also distributed on LDs and ER membranes[10,21,27], DCV-mediated disruption of NS5A membrane-association on these interfaces may subsequently inhibit RNA transfer, which could require NS5A multimers to guide HCV RNA towards structural proteins, as proposed elsewhere[1,6,34-36]. Thus, regardless of NS5A localization, this would explain why DCV did not alter RNA/NS5A colocalization (Figure 6) as DCV does not inhibit RNA/NS5A binding[14,29], whereas perturbing NS5A multimers by DCV, *via* either their disruption or altered membrane association, would likely have a strong impact on RNA transfer and packaging in assembling virions. Third, DCV-induced perturbation of NS5A amino-terminus, which interacts with NS4B C-terminal domain (CTD)[40,41], may preclude NS4B packaging functions[42] and RNA transfer to core. In this respect, it is interesting to note that DCV treatment also strongly reduced the colocalization of NS4B and HCV RNA(+) strand (Figure 6). This likely reflects the role of NS4B in post-replication steps[32,43], particularly the packaging function of its CTD[42] that relies both on weak RNA binding capacity[44] and on interaction with the DIII domain of NS5A that is involved in HCV assembly[18,38,39,45].

Interestingly, enlarged E2/core/NS5A and E2/core/NS4B structures were observed for the Y93H DCV-resistant virus as compared to WT in absence of DCV (Figures 1 and 2). Nonetheless, RNA(+) dots readily localized with core or NS4B structures (Figure 6B), even in the presence of DCV (Supplemental Figure 1), congruent with efficient viral particle assembly of this mutant. Therefore, in line with the above-discussed model, we propose that DCV-escape mutations may compensate altered membranotropic properties of NS5A and

optimize interactions with NS4B (and/or other non-structural proteins) in order to maintain efficient RNA targeting to assembly sites. Additional experiments will be required to validate this hypothesis.

In conclusion, our results indicate that DCV may inhibit HCV by preventing NS5A-mediated HCV RNA transfer to sites of virion assembly, in addition to other effects induced by this multifunctional protein[8]. This finding emphasizes the attractiveness of this class of inhibitors that target two distinct steps of HCV cycle, *i.e.*, RNA replication and viral particle assembly. Furthermore, investigating the mode of action of DCV allowed to further characterize how replication and assembly are intimately linked and what is a specific function of NS5A in this respect.

Supplementary Material

To access the supplementary material accompanying this article, visit the online version of Gastroenterology at www.gastrojournal.org, and at …
Supplementary Material includes Supplementary Materials and Methods, Supplemental Results and nine Supplemental Figures.

References

1. Bartenschlager R, Lohmann V, Penin F. The molecular and structural basis of advanced antiviral therapy for hepatitis C virus infection. Nat Rev Microbiol 2013;11:482-96.
2. Gotte M, Feld JJ. Direct-acting antiviral agents for hepatitis C: structural and mechanistic insights. Nat Rev Gastroenterol Hepatol 2016;13:338-51.
3. Gao M, Nettles RE, Belema M, et al. Chemical genetics strategy identifies an HCV NS5A inhibitor with a potent clinical effect. Nature 2010;465:96-100.
4. Guedj J, Dahari H, Rong L, et al. Modeling shows that the NS5A inhibitor daclatasvir has two modes of action and yields a shorter estimate of the hepatitis C virus half-life. Proc Natl Acad Sci U S A 2013;110:3991-6.
5. McGivern DR, Masaki T, Williford S, et al. Kinetic analyses reveal potent and early blockade of hepatitis C virus assembly by NS5A inhibitors. Gastroenterology 2014;147:453-62 e7.
6. Berger C, Romero-Brey I, Radujkovic D, et al. Daclatasvir-like inhibitors of NS5A block early biogenesis of hepatitis C virus-induced membranous replication factories, independent of RNA replication. Gastroenterology 2014;147:1094-105 e25.
7. Ascher DB, Wielens J, Nero TL, et al. Potent hepatitis C inhibitors bind directly to NS5A and reduce its affinity for RNA. Sci Rep 2014;4:4765.
8. Ross-Thriepland D, Harris M. Hepatitis C virus NS5A: enigmatic but still promiscuous 10 years on! J Gen Virol 2015;96:727-38.

9. Chatterji U, Bobardt M, Tai A, et al. Cyclophilin and NS5A inhibitors, but not other anti-hepatitis C virus (HCV) agents, preclude HCV-mediated formation of double-membrane-vesicle viral factories. Antimicrob Agents Chemother 2015;59:2496-507.
10. Romero-Brey I, Merz A, Chiramel A, et al. Three-dimensional architecture and biogenesis of membrane structures associated with hepatitis C virus replication. PLoS Pathog 2012;8:e1003056.
11. Romero-Brey I, Berger C, Kallis S, et al. NS5A Domain 1 and Polyprotein Cleavage Kinetics Are Critical for Induction of Double-Membrane Vesicles Associated with Hepatitis C Virus Replication. MBio 2015;6:e00759.
12. Chukkapalli V, Berger KL, Kelly SM, et al. Daclatasvir inhibits hepatitis C virus NS5A motility and hyper-accumulation of phosphoinositides. Virology 2015;476:168-79.
13. Lee C, Ma H, Hang JQ, et al. The hepatitis C virus NS5A inhibitor (BMS-790052) alters the subcellular localization of the NS5A non-structural viral protein. Virology 2011;414:10-8.
14. Targett-Adams P, Graham EJ, Middleton J, et al. Small molecules targeting hepatitis C virus-encoded NS5A cause subcellular redistribution of their target: insights into compound modes of action. J Virol 2011;85:6353-68.
15. Reghellin V, Donnici L, Fenu S, et al. NS5A inhibitors impair NS5A-phosphatidylinositol 4-kinase IIIalpha complex formation and cause a decrease of phosphatidylinositol 4-phosphate and cholesterol levels in hepatitis C virus-associated membranes. Antimicrob Agents Chemother 2014;58:7128-40.
16. Huang L, Hwang J, Sharma SD, et al. Hepatitis C virus nonstructural protein 5A (NS5A) is an RNA-binding protein. J Biol Chem 2005;280:36417-28.
17. Foster TL, Belyaeva T, Stonehouse NJ, et al. All three domains of the hepatitis C virus nonstructural NS5A protein contribute to RNA binding. J Virol 2010;84:9267-77.
18. Zayas M, Long G, Madan V, et al. Coordination of Hepatitis C Virus Assembly by Distinct Regulatory Regions in Nonstructural Protein 5A. PLoS Pathog 2016;12:e1005376.
19. Pietschmann T, Kaul A, Koutsoudakis G, et al. Construction and characterization of infectious intragenotypic and intergenotypic hepatitis C virus chimeras. Proc Natl Acad Sci U S A 2006;103:7408-13.
20. Boson B, Granio O, Bartenschlager R, et al. A concerted action of hepatitis C virus p7 and nonstructural protein 2 regulates core localization at the endoplasmic reticulum and virus assembly. PLoS Pathog 2011;7:e1002144.
21. Miyanari Y, Atsuzawa K, Usuda N, et al. The lipid droplet is an important organelle for hepatitis C virus production. Nat Cell Biol 2007;9:1089-97.
22. Qiu D, Lemm JA, O'Boyle DR, 2nd, et al. The effects of NS5A inhibitors on NS5A phosphorylation, polyprotein processing and localization. J Gen Virol 2011;92:2502-11.
23. Fridell RA, Qiu D, Valera L, et al. Distinct functions of NS5A in hepatitis C virus RNA replication uncovered by studies with the NS5A inhibitor BMS-790052. J Virol 2011;85:7312-20.
24. Shavinskaya A, Boulant S, Penin F, et al. The lipid droplet binding domain of hepatitis C virus core protein is a major determinant for efficient virus assembly. J Biol Chem 2007;282:37158-69.
25. Boulant S, Targett-Adams P, McLauchlan J. Disrupting the association of hepatitis C virus core protein with lipid droplets correlates with a loss in production of infectious virus. J Gen Virol 2007;88:2204-13.
26. Herker E, Harris C, Hernandez C, et al. Efficient hepatitis C virus particle formation requires diacylglycerol acyltransferase-1. Nat Med 2010;16:1295-8.
27. Camus G, Herker E, Modi AA, et al. Diacylglycerol acyltransferase-1 localizes hepatitis C virus NS5A protein to lipid droplets and enhances NS5A interaction with the viral capsid core. J Biol Chem 2013;288:9915-23.
28. Shulla A, Randall G. Spatiotemporal analysis of hepatitis C virus infection. PLoS Pathog 2015;11:e1004758.

29. Nag A, Robotham JM, Tang H. Suppression of viral RNA binding and the assembly of infectious hepatitis C virus particles in vitro by cyclophilin inhibitors. J Virol 2012;86:12616-24.
30. Kim N, Kim MJ, Sung PS, et al. Interferon-inducible protein SCOTIN interferes with HCV replication through the autolysosomal degradation of NS5A. Nat Commun 2016;7:10631.
31. Madan V, Paul D, Lohmann V, et al. Inhibition of HCV replication by cyclophilin antagonists is linked to replication fitness and occurs by inhibition of membranous web formation. Gastroenterology 2014;146:1361-72 e1-9.
32. Paul D, Romero-Brey I, Gouttenoire J, et al. NS4B self-interaction through conserved C-terminal elements is required for the establishment of functional hepatitis C virus replication complexes. J Virol 2011;85:6963-76.
33. Gouttenoire J, Montserret R, Paul D, et al. Aminoterminal amphipathic alpha-helix AH1 of hepatitis C virus nonstructural protein 4B possesses a dual role in RNA replication and virus production. PLoS Pathog 2014;10:e1004501.
34. Appel N, Schaller T, Penin F, et al. From structure to function: new insights into hepatitis C virus RNA replication. J Biol Chem 2006;281:9833-6.
35. Lambert SM, Langley DR, Garnett JA, et al. The crystal structure of NS5A domain 1 from genotype 1a reveals new clues to the mechanism of action for dimeric HCV inhibitors. Protein Sci 2014;23:723-34.
36. Love RA, Brodsky O, Hickey MJ, et al. Crystal structure of a novel dimeric form of NS5A domain I protein from hepatitis C virus. J Virol 2009;83:4395-403.
37. Paul D, Hoppe S, Saher G, et al. Morphological and biochemical characterization of the membranous hepatitis C virus replication compartment. J Virol 2013;87:10612-27.
38. Masaki T, Suzuki R, Murakami K, et al. Interaction of hepatitis C virus nonstructural protein 5A with core protein is critical for the production of infectious virus particles. J Virol 2008;82:7964-76.
39. **Appel N, Zayas M**, Miller S, et al. Essential role of domain III of nonstructural protein 5A for hepatitis C virus infectious particle assembly. PLoS Pathog 2008;4:e1000035.
40. Biswas A, Treadaway J, Tellinghuisen TL. Interaction Between Non-Structural Proteins NS4B And NS5A Is Essential For Proper NS5A Localization And Hepatitis C Virus RNA Replication. J Virol 2016;90:7205-18.
41. David N, Yaffe Y, Hagoel L, et al. The interaction between the hepatitis C proteins NS4B and NS5A is involved in viral replication. Virology 2015;475:139-49.
42. Han Q, Manna D, Belton K, et al. Modulation of hepatitis C virus genome encapsidation by nonstructural protein 4B. J Virol 2013;87:7409-22.
43. Jones DM, Patel AH, Targett-Adams P, et al. The hepatitis C virus NS4B protein can trans-complement viral RNA replication and modulates production of infectious virus. J Virol 2009;83:2163-77.
44. **Einav S, Gerber D**, Bryson PD, et al. Discovery of a hepatitis C target and its pharmacological inhibitors by microfluidic affinity analysis. Nat Biotechnol 2008;26:1019-27.
45. Tellinghuisen TL, Foss KL, Treadaway JC, et al. Identification of residues required for RNA replication in domains II and III of the hepatitis C virus NS5A protein. J Virol 2008;82:1073-83.

Author names in bold designate shared co-first authorship.

Figure legends

Figure 1. Daclatasvir induces the clustering of E2/core/NS5A structures. Huh7.5 cells infected with Jc1 or Jc1-Y93H viruses (MOI=0.2) were incubated at 66h post-infection with 1nM of DCV or DMSO for 6h. Following staining for HCV E2, core and NS5A proteins, colocalization of core (red channel) with E2 (green channel) and NS5A (blue channel) proteins was analyzed by confocal microscopy (**A**). Scale bars of panels and zooms from squared area represent 10µm and 2µm, respectively. Colocalized pixels (white channel) between red, green and blue channels were extracted with the ColocalizeRGB plugin of ImageJ. The surface (**B**) and number (**C**) of E2/core/NS5A and core/NS5A structures were quantified with ImageJ. For each condition, 30-50 cells were quantified.

Figure 2. Daclatasvir induces the clustering of E2/core/NS4B structures. Cells were infected, treated and analyzed as in Figure 1. Confocal analysis of core with E2 and NS4B, displayed as in Figure 1A, with NS4B instead of NS5A in the blue channel (**A**). The surface (**B**) and number (**C**) of E2/core/NS4B and core/NS4B structures were quantified with ImageJ.

Figure 3. 3D-SIM Super-Resolution imaging of E2/core/NS4B structures. Cells were infected with Jc1 virus (MOI=0.2), treated for 24h with 20µg/mL cycloheximide at 48h post-infection, and fixed at 72h post-infection. Cells were stained for HCV E2, core and NS4B proteins and for LDs. Colocalization of core (red channel) with E2 (green channel) and NS4B (blue channel) (**A**) or core with LDs (green channel) and NS4B (blue channel) (**B**) was analyzed by 3D-SIM. Zooms of typical structures are represented as individual stack from top to bottom (referred to 1 to 10) and 3D-reconstructions from Imaris software are shown. Scale bars of panels and zooms from squared area represent 5µm and 1µm, respectively.

Figure 4. Structural proteins and NS4B colocalize within discrete structures. Cells infected with Jc1 or JFH1 viruses (MOI=0.2) were fixed at the indicated time post-infection and were then stained for HCV E2, core and NS4B proteins. The colocalization of core (red channel) with E2 (green channel) and NS4B (blue channel) was analyzed by confocal microscopy. A representative picture of Jc1-infected cells is presented (**A**). Scale bars of panels and zooms from squared area represent 10µm and 2µm, respectively. Colocalized pixels (white channel) between red, green and blue channels were extracted with the ColocalizeRGB plugin of ImageJ (second row). The number (**B**) and size (**C**) of E2/core/NS4B structures were quantified with ImageJ. For each condition, 30-50 cells were quantified. The supernatants of infected cells were harvested at the indicated time post-infection and used to infect naïve Huh7.5 cells to determine virus infectivity (**D**).

Figure 5. Characterization of HCV core structures within infected cells. A schematic representation distinguishing the different categories of core structures with regard to LD localization that were quantified (**A**). From images of Supplemental Figure 8A, the percentage of core punctate structures apposed at the edge of LDs (**B**) and the percentage of LDs with associated core either on ER membrane or on LD surface (**C**) were quantified using a macro developed with ImageJ (see Supplemental Results). The percentage of core/NS4B and core/NS5A punctate structures apposed at the edge of LDs in Jc1-infected cells (**D**) were quantified with ImageJ. ND, not determined. For each condition, 30-50 cells were quantified.

Figure 6. Daclatasvir prevents the delivery of HCV RNA(+) to assembly sites. Cells infected with Jc1 or Jc1-Y93H viruses (MOI=0.2) were incubated at 66h post-infection with 1nM of DCV or DMSO for 6h. Following staining for HCV core, NS4B and NS5A proteins and nuclei, HCV RNA(+) and RNA(-) species were stained by fluorescent *in situ* hybridization. Colocalization of core (red channel) with NS4B or NS5A proteins (green channel) and HCV RNA(+) or RNA(-) strands (blue channel) was analyzed by confocal microscopy (**A**). Nuclei are represented as cyan channel. Scale bars of panels and zooms from squared area represent 10µm and 2µm, respectively. The proportion of core/NS4B and core/NS5A colocalizing with HCV RNA(+) (**B**) or RNA(-) (**C**), as well as the proportion of HCV RNA(+) (**B**) or RNA(-) (**C**) dots colocalizing with core, NS4B or NS5A structures were quantified with ImageJ. For each condition, 30-50 cells were quantified.

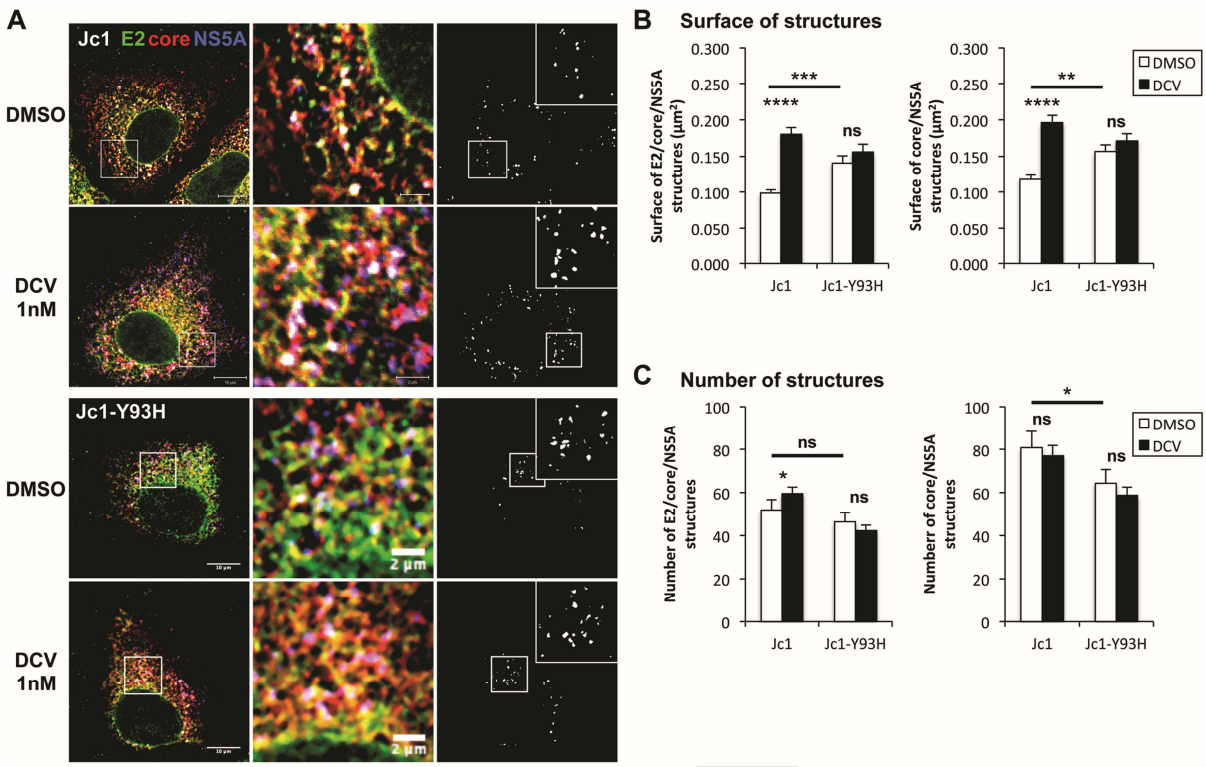

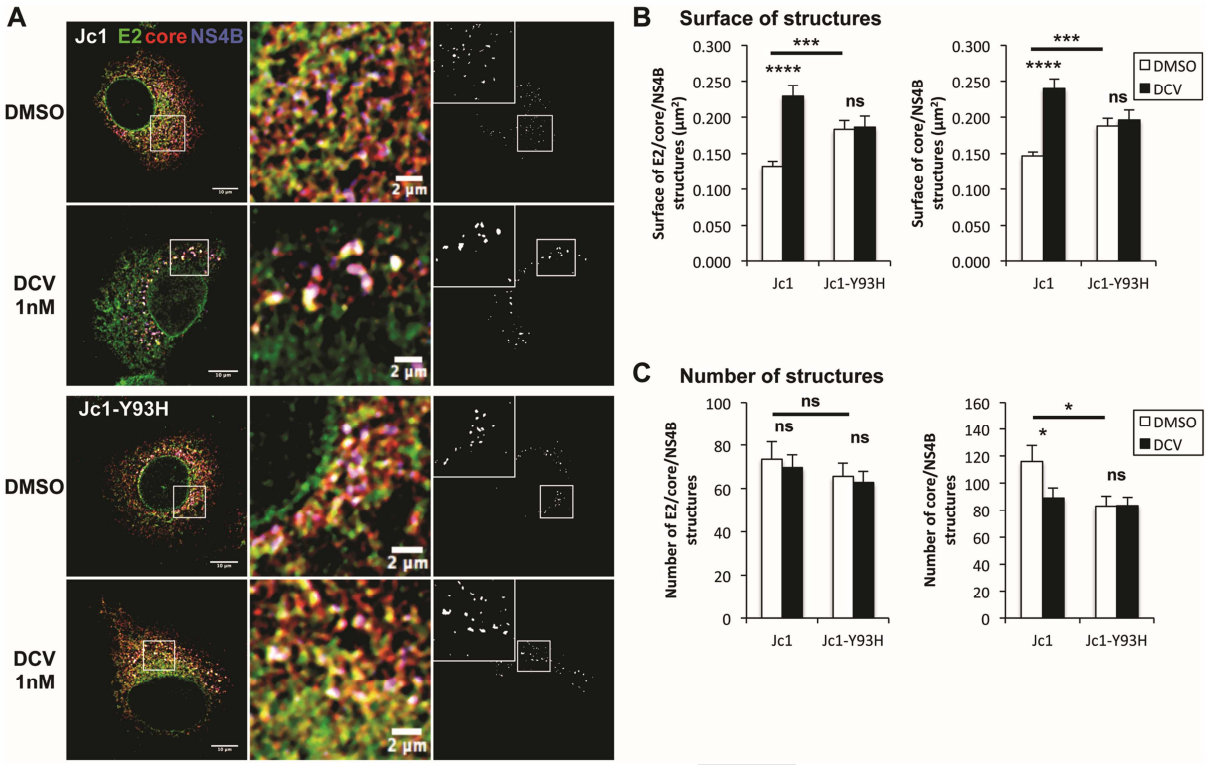

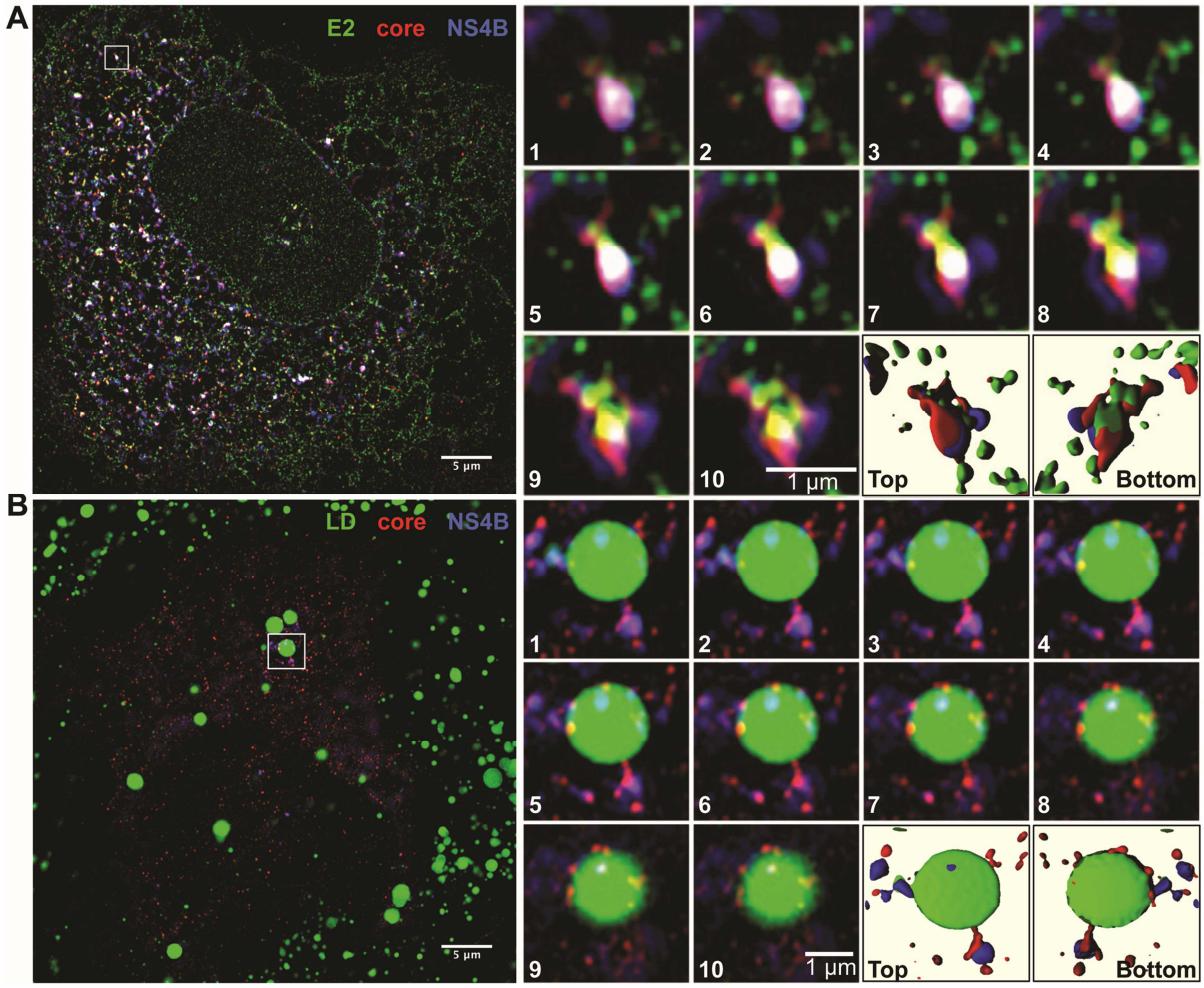
A
E2 core NS4B
5 μm
1
2
3
4
5
6
7
8
9
10
1 μm
Top
Bottom
B
LD core NS4B
5 μm
1
2
3
4
5
6
7
8
9
10
1 μm
Top
Bottom

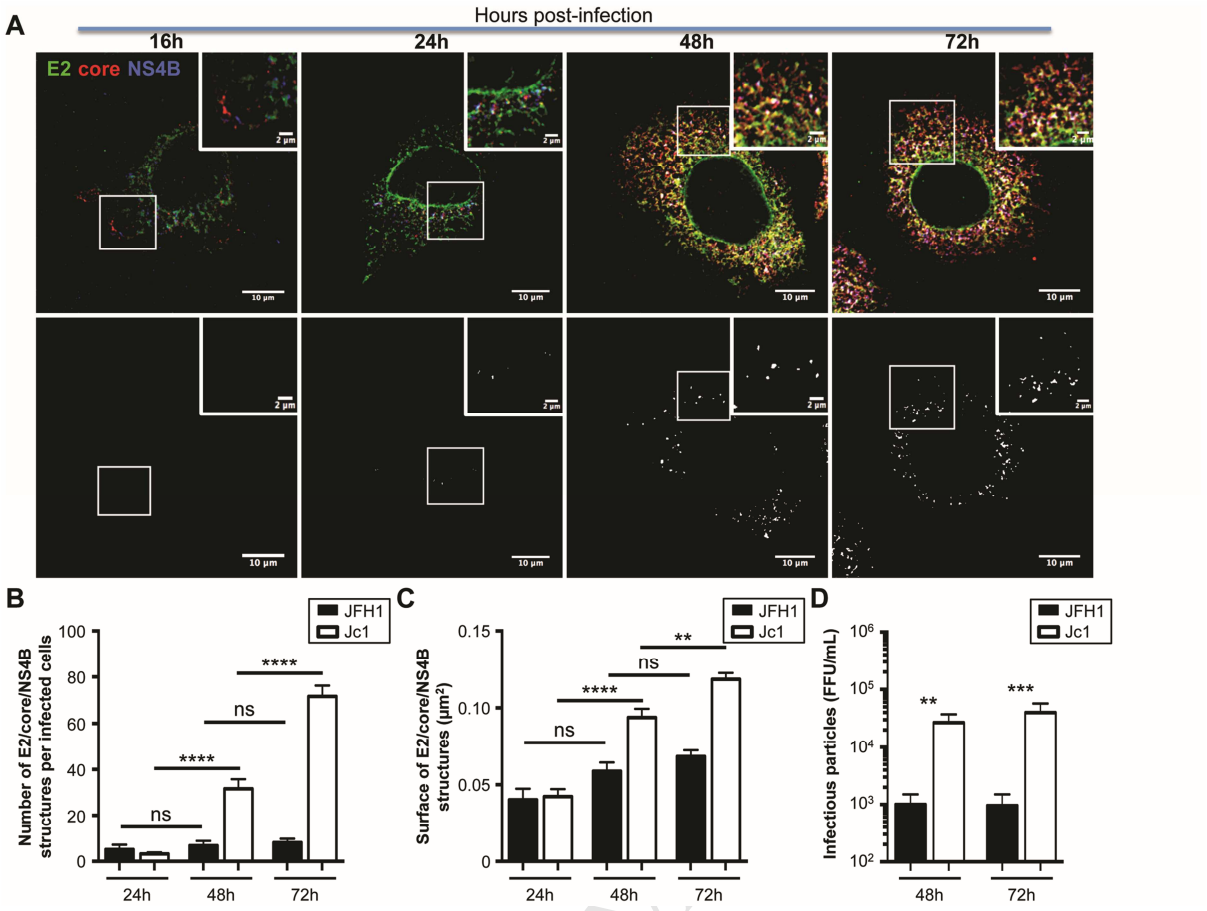

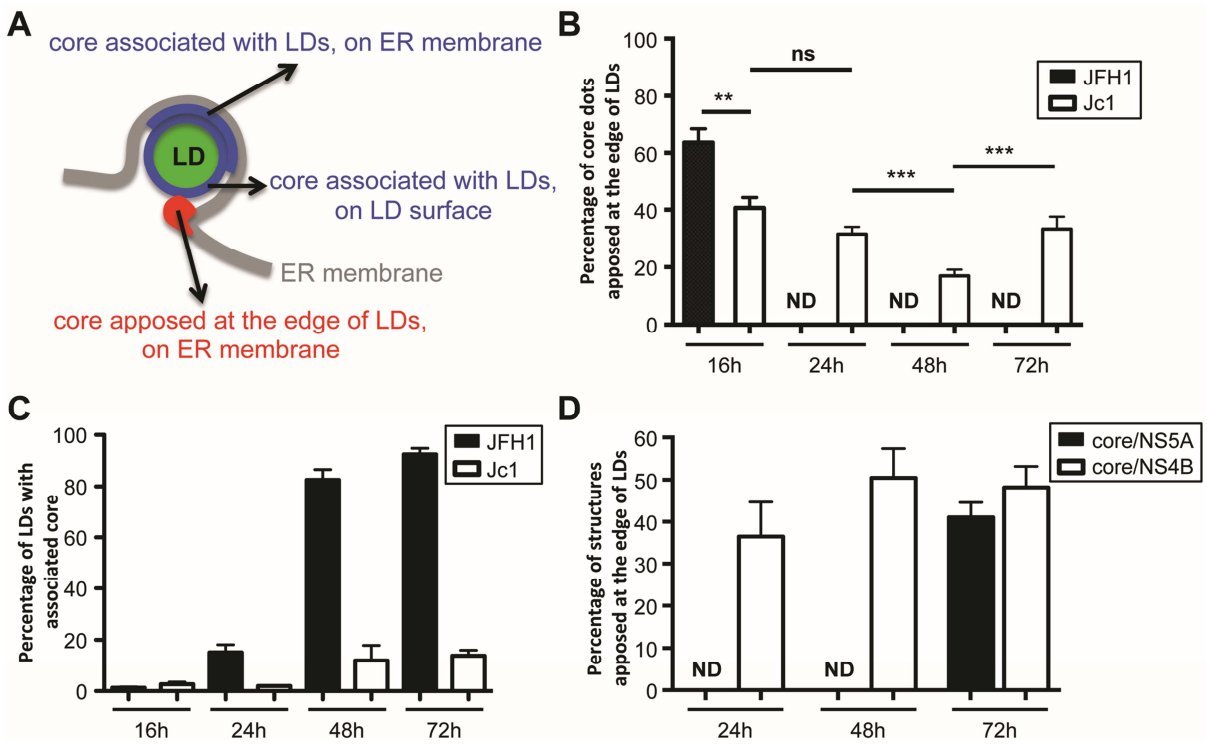

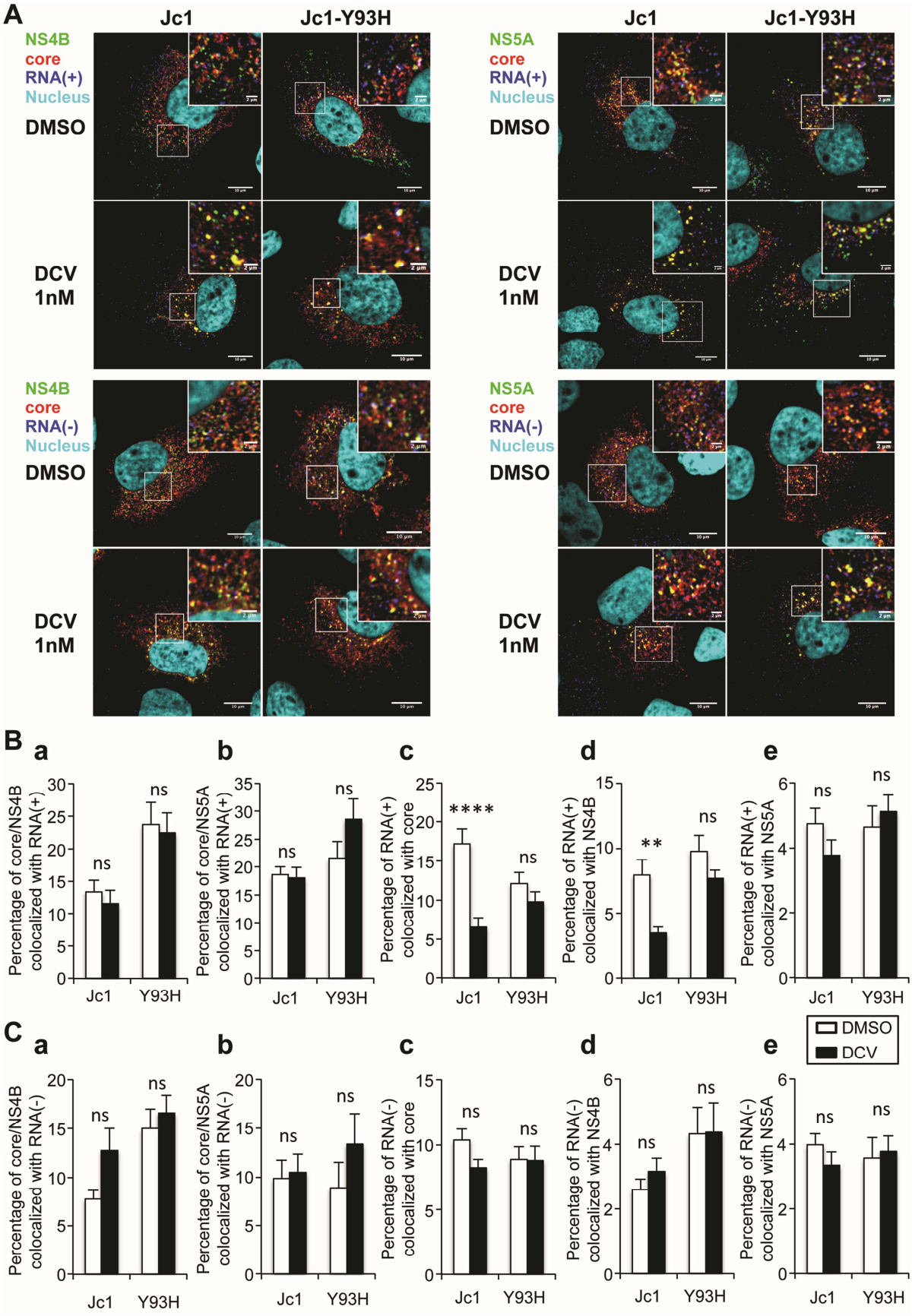
A
Jc1
Jc1-Y93H
NS4B
core
RNA(+)
Nucleus
DMSO
DCV
1nM
NS5A
core
RNA(+)
Nucleus
DMSO
DCV
1nM
NS4B
core
RNA(-)
Nucleus
DMSO
DCV
1nM
NS5A
core
RNA(-)
Nucleus
DMSO
DCV
1nM
B
a
Percentage of core/NS4B colocalized with RNA(+)
b
Percentage of core/NS5A colocalized with RNA(+)
c
Percentage of RNA(+) colocalized with core
d
Percentage of RNA(+) colocalized with NS4B
e
Percentage of RNA(+) colocalized with NS5A
ns
****
**
Jc1
Y93H
C
a
Percentage of core/NS4B colocalized with RNA(-)
b
Percentage of core/NS5A colocalized with RNA(-)
c
Percentage of RNA(-) colocalized with core
d
Percentage of RNA(-) colocalized with NS4B
e
Percentage of RNA(-) colocalized with NS5A
DMSO
DCV

GASTRO-D-16-01378 Revised

Supplemental Material

Unraveling the mode of action of the NS5A inhibitor Daclatasvir on hepatitis C virus assembly

Short title: DCV impairs HCV RNA transfer to assembly site

Authors: Bertrand Boson[1], Solène Denolly[1], Fanny Turlure[1], Christophe Chamot[2], Marlène Dreux[1], François-Loïc Cosset[1]

[1]CIRI – International Center for Infectiology Research, Team EVIR, Inserm, U1111, Université Claude Bernard Lyon 1, CNRS, UMR5308, Ecole Normale Supérieure de Lyon, Univ Lyon, F-69007, Lyon, France.
[2]PLATIM, US8 / UMS3444 BioSciences Gerland, Lyon, France.

Funding: This work was supported by the French “Agence Nationale de la Recherche sur le SIDA et les hépatites virales” (ANRS), the European Research Council (ERC-2008-AdG-233130-HEPCENT) and the LabEx Ecofect (ANR-11-LABX-0048).

Abbreviations: HCV, hepatitis C virus; DCV, Daclatasvir; RNA, ribonucleic acid; RC, replication complex; DAA, direct-acting antiviral; NS, nonstructural protein; EC, effective concentration; DMV, double membrane vesicle; FFU, focus-forming unit; MOI, multiplicity of infection; CHX, cycloheximide; ER, endoplasmic reticulum; LD, lipid droplet; SIM, Structured Illumination Microscopy; DGAT1, diacylglycerol acyltransferase-1; FISH, Fluorescent *In-Situ* Hybridization; GE, genome equivalent; ns, not significant; ND, not determined; CTD, C-terminal domain.

To whom correspondence should be addressed: François-Loïc Cosset. CIRI – International Center for Infectiology Research, Team EVIR, Université de Lyon, Lyon, France. E-mail: flcosset@ens-lyon.fr

Supplemental Materials and Methods

Antibodies and reagents. Rabbit antiserum against Calnexin (Sigma Aldrich, France), mouse anti-ADRP (clone AP125, Progen, Heidelberg, Germany), mouse anti-Actin (clone AC74, Sigma Aldrich, France), rabbit anti-DGAT1 (clone H-255, Santa Cruz Biotechnology, USA), mouse anti-core 19D9D6 (kind gift from C. Jolivet, bioMérieux, Lyon, France), rat anti-E2 clone 3/11 (kind gift from J. McKeating, University of Birmingham, UK), mouse anti-NS5A 9E10 (kind gift from C. Rice, Rockefeller University, New York, USA), rabbit anti-NS4B (kind gift from M. Kohara, Tokyo Metropolitan Institute of Medical Science, Tokyo, Japan), Daclatasvir (BMS-790052, Selleck Chemicals, USA), A922500 (Sigma Aldrich, France), Cycloheximide (Sigma Aldrich, France), Mowiol 40-88 (Fluka, Switzerland), Bodipy 493/503 and Hoecsht 33342 (Molecular Probes Europe BV, The Netherlands), Fluoromount-G (SouthernBiotech, USA), Protease/Phosphatase Inhibitor Cocktail (Cell Signaling Technology, USA) were used according to the manufacturer's instructions.

Inhibition of diacylglycerol acyltransferase-1 (DGAT1). Down-regulation of DGAT1 was achieved using procedure previously described[1] *via* a small interfering RNA (5'-GAACCTCATCAAGTATGGCAT) expressed from a lentiviral vector (MISSION pLKO.1-puro vector with shRNA insert TRCN0000036153, Sigma-Aldrich, France). DGAT1 expression was verified by Western blot analysis. Inhibition of DGAT1 was achieved using 150µM of A922500 inhibitor added at the time of infection for 72h.

Analysis of intracellular and extracellular RNA levels. RNAs were isolated from cells and supernatant harvested in guanidinium thiocyanate citrate buffer (GTC), extracted by phenol/chloroform extraction, reverse transcribed (iScript cDNA synthesis kit, Bio-Rad, USA), and quantified with the FastStart Universal SYBR Green Master kit (Roche Applied Science, USA) on an Applied StepOne Real-Time PCR apparatus, as described previously[2,3]. The efficiency of extracellular RNA extraction and reverse transcription-real-time quantitative PCR (RT-qPCR) was controlled by the addition of carrier RNAs encoding *in vitro* transcripts of Xef1a (xenopus transcription factor 1a) in supernatants diluted in GTC buffer. The sequences of the primers used for the RT-qPCR were: HCV-specific primers (5′-CTGCGGAACCGGTGAGTA and 5′-TCAGGCAGTACCACAAGGC), glyceraldehyde-3-phosphate dehydrogenase (GAPDH)-specific primers (5'-AGGTGAAGGTCGGAGTCAACG and 5'-TGGAAGATGGTGATGGGATTTC), and Xef1a-specific primers (5'-GACGTTGTCAC CGGGCACG and 5'-ACCAGGCATGGTGGTTACCTT TGC). Extracellular and intracellular HCV RNA levels were normalized for Xef1a and GAPDH RNA levels, respectively.

Analysis of intracellular and extracellular core protein levels. Infected cells were washed with PBS, trypsinized and centrifuged for 5min at 400xg. Cell pellets were resuspended in PBS and subjected to four cycles of freeze and thaw using liquid nitrogen. Samples were then centrifuged at 10,000xg for 10min to remove cell debris. For the quantification of extracellular core protein levels, supernatants of infected cells were harvested and diluted in DMEM to obtain a final concentration of 5% BSA. Core protein levels were then quantified with the HCV core Antigen Detection ELISA assay (XpressBio, USA) according to the manufacturer's instructions.

Subcellular fractionation. Separation of different membrane compartments was achieved as described previously[4]. Huh7.5 cells were electroporated with *in vitro* transcribed Jc1 RNA. 66h post-electroporation, cells were washed three times and were incubated with 1nM DCV or DMSO for an additional 6h. Cells were then detached, washed in PBS and homogenized in 1 volume of 10mM Hepes-NaOH 10mM pH 7.8 (hypo-osmotic buffer). Cells were allowed to swell on ice for 20min and were re-isolated by centrifugation at 800xg at 4℃ for 5min. The medium was returned to iso-osmoticity by removing 2/3rd of the supernatant and adding 1/3rd volume of 0.6M sucrose, 10mM Hepes-NaOH at pH 7.8 (hyper-osmotic buffer). Cells were disrupted by passaging 20 times through a 25 G needle and lysates were extracted from the nuclei by centrifugation at 13,000xg for 10min at 4℃. Subcellular fractionation was performed in three-step iodixanol gradients. Equal protein amounts of the post-nuclear extracts (PNE) were mixed with 60% iodixanol to give a final concentration of 30%, the hypo-osmotic buffer was mixed with 60% iodixanol to generate 10% and 20% iodixanol solutions. Equal volumes of these three solutions were layered in SW60Ti centrifuge tubes and centrifuged at 50krpm for 3h at 4℃. 12 fractions were collected from the top and proteins were revealed by Western blotting.

Western blotting. Infected cells were lysed in lysis buffer (20mM Tris pH7.5, 1% TritonX100, 0.05% SDS, 150nM NaCL, 5‰ Na Deoxycholate) supplemented with protease/phosphatase inhibitor cocktail (Cell Signaling Technology, USA) and clarified from the nuclei by centrifugation at 13,000xg for 10min at 4℃. 10µg of total proteins were separated by SDS-polyacrylamide gel electrophoresis (PAGE), then transferred to polyvinylidene fluoride membranes (FluoroTrans W, Pall Corporation, USA) and revealed with specific monoclonal antibodies, followed by the addition of goat anti-mouse, anti-rat or anti-rabbit immunoglobulin conjugated to peroxydase (Dako A/S, Denmark). The proteins of interest were revealed by enhanced chemiluminescence detection (SuperSignal® West Pico Chemiluminescent, Thermo Scientific, USA) as recommended by the manufacturer.

Supplemental Results

For quantification of structures apposed at the edge of LDs[5], we developed an ImageJ macro that searches for variation of max intensity in the neighborhood of each LD as an indicator of proximity. The code of this macro is shown below:

showMessage("The system will now search for variation of \nmax intensity in the neighborhood of each vesicle\nas indicator of proximity\n\nThe integrated density should increase dramatically too.");

```
//Image management
if (nImages==0) {
        exit("No images are open");
 }else{
        getDimensions(width, height, channels, slices, frames);
        if(channels>1)  run("Split Channels");
        titres=newArray(nImages);
        //setBatchMode(true);
        for (i=1; i<=nImages; i++) {
        selectImage(i);
        titres[i-1]=getTitle();
    }

dir=getDirectory("image");

Dialog.create("Parameters");
Dialog.addNumber("Number of dilatations", 3);
Dialog.addNumber("Max. variation of max intensity", 50);
Dialog.addNumber("Max. variation of integrated intensity", 2000);
Dialog.addNumber("Min. area for analysis", 0.02);
Dialog.addChoice("To dilate", titres);
Dialog.addChoice("Target", titres);
Dialog.addCheckbox("Save ROIs ?", 0);
Dialog.show();
n=Dialog.getNumber();
maxIntVar=Dialog.getNumber();
```

```
maxDenVar=Dialog.getNumber();
minArea=Dialog.getNumber();
toDilate=Dialog.getChoice();
target=Dialog.getChoice();
saveROI=Dialog.getCheckbox();


//Preparation and configuration
run("Set Measurements...", "area min integrated redirect=None decimal=3");
roiManager("reset");

//Removing of channels useless for this analysis and separation of channels
/*setSlice(2);
run("Delete Slice", "delete=channel");
run("Next Slice [>]");
run("Delete Slice", "delete=channel");
run("Split Channels");
*/

/* TODO add sequence of automatic selection of the cell
run("Next Slice [>]");
run("Gaussian Blur...", "sigma=20 slice");
setAutoThreshold("Percentile dark");
setAutoThreshold("Percentile dark");
run("Convert to Mask");
doWand(265, 252);
*/

//Automatic thresholding and separation
selectImage(toDilate);

//Possibility to place a ROI around the cell
waitForUser("Place ROI around the cell to avoid\nexternal counting");

//ROI counting
selectImage(toDilate);
```

```
run("Analyze Particles...", "size="+minArea+"-Infinity circularity=0.00-1.00 show=Nothing add");

//Selection of the image carrying the information
selectImage(target);
//selectWindow("C1-Jc1LDcoreNS4B4.lsm");

//Highlighting of the counted areas
roiManager("Show All without labels");

//Saving of the ROI

if(saveROI) roiManager("Save", "");

//Scanning of the ROI
for(i=0;i<roiManager("count");i++){
roiManager("Select", i);
	//Measure of the dilations
	j=1;
	while(j<=n){
		run("Measure");
		run("Enlarge...", "enlarge=1 pixel");
		j++;
		}//end of ROI measurement

		//Construction secondary tables
		//Table of max
		maxs=newArray(n);
		for(z=0;z<n;z++){
			maxs[z]=getResult("Max", z);
		}
		/*Array.print(maxs);
		print(maxs[4]);
		Array.reverse(maxs);
		Array.print(maxs);
		print(maxs[4]);
		Array.getStatistics(maxs, min, max, mean, stdDev);
```

```
                print(stdDev);
                print(delta(maxs))
                */

                //Table of integrated intensities
                intDen=newArray(n);
                for(y=0;y<n;y++){
                        intDen[y]=getResult("RawIntDen", y);
                }

                //Decision of the positive character or not
        if((delta(maxs)>maxIntVar)||(delta(intDen)>maxDenVar)) {
        print("ROI "+i+1+"\tpositif");
        }else{
                print("ROI "+i+1+"\tnegatif");
        }
           //if(deltaMax<threshold) the area of max intensity is close by
           //if(deltaRawIntDen>threshold) progress thus closeness

           //deletion of n first rows of the table
           IJ.deleteRows(0, n-1);


}//end of the scanning of the ROI

function delta(a){
val=0;
for(i=1;i<a.length;i++){
        val=val+a[i]-a[i-1];
        }
return val;
}
```

Supplementary References

1. Lavillette D, Tarr AW, Voisset C, et al. Characterization of host-range and cell entry properties of hepatitis C virus of major genotypes and subtypes. Hepatology 2005;41:265-274.
2. Calattini S, Fusil F, Mancip J, et al. Functional and Biochemical Characterization of Hepatitis C Virus (HCV) Particles Produced in a Humanized Liver Mouse Model. J Biol Chem 2015;290:23173-87.
3. Dao Thi VL, Granier C, Zeisel MB, et al. Characterization of hepatitis C virus particle subpopulations reveals multiple usage of the scavenger receptor BI for entry steps. J Biol Chem 2012;287:31242-57.
4. Boson B, Granio O, Bartenschlager R, et al. A concerted action of hepatitis C virus p7 and nonstructural protein 2 regulates core localization at the endoplasmic reticulum and virus assembly. PLoS Pathog 2011;7:e1002144.
5. Boulant S, Targett-Adams P, McLauchlan J. Disrupting the association of hepatitis C virus core protein with lipid droplets correlates with a loss in production of infectious virus. J Gen Virol 2007;88:2204-13.

Supplemental Figure legends

Supplemental Figure 1. Daclatasvir prevents HCV assembly. Huh7.5 cells infected with Jc1 or Jc1-Y93H viruses (MOI=0.2) were incubated 66h post-infection with 1nM of DCV or DMSO for 6h *vs*. 24h, as outlined in the boxed panel. (**A**) The intracellular viral genomes (left panels) and core proteins (right panel) were quantified by RT-qPCR and ELISA, respectively. (**B**) The intracellular or extracellular infectivity was determined from cell lysates or supernatants of infected cells, respectively. (**C**) The extracellular physical particles were analyzed by quantification of the release of viral RNA (left panel) or core protein (right panel) in the supernatant by RT-qPCR and ELISA, respectively. GE, genome equivalent. ****, P≤0.0001; ***, P≤0.001; **, P≤0.01; *, P≤0.05; ns (not significant), P>0.05.

Supplemental Figure 2. HCV assembly inhibition by Daclatasvir correlates with clustering of structural proteins and NS4B. Huh7.5 cells were infected with Jc1 or Jc1-Y93H viruses at an MOI of 0.2. At 66h post-infection, cells were washed and incubated with 1nM of DCV or DMSO for the indicated time, as outlined in the boxed panel. (**A**) The intracellular and (**B**) the extracellular infectivity were determined from cell lysates or supernatants of infected cells, respectively. (**C**) The size and (**D**) the number of E2/core/NS4B structures were quantified with ImageJ. For each timepoint, results are expressed as percentage of the value at the initiation of DCV treatment (T0). For each condition, 30-50 cells were quantified. ****, P≤0.0001; ***, P≤0.001; **, P≤0.01; *, P≤0.05; ns (not significant), P>0.05.

Supplemental Figure 3. Jc1 core punctate structures colocalize with E2 and elements of the replication complexes. Huh7.5 cells were infected with Jc1 virus at an MOI of 0.2, treated for 24h with 20µg/mL of cycloheximide at 48h post-infection, and fixed at 72h post-infection. Cells were stained for HCV core and other viral proteins, as indicated. (**A**) Colocalization of core (red channel) with E2 or NS2 or NS3 or NS4B or NS5A (green channel) was analyzed by confocal microscopy. Scale bars of panels and zooms from squared area represent 10µm and 2µm, respectively. (**B**) The relative degree of colocalization of proteins was quantified by determining Pearson's correlation coefficients of 20 cells by using the JACoP plugin of ImageJ.

Supplemental Figure 4. Daclatasvir induces the clustering of core/NS4B/NS5A structures. Huh7.5 cells infected with Jc1 or Jc1-Y93H viruses (MOI=0.2) were incubated at 66h post-infection with 1nM of DCV or DMSO for 6h. (**A**) Cells were then stained for HCV core, NS4B and NS5A proteins and the colocalization of core (red channel) with NS4B

(green channel) and NS5A (blue channel) proteins was analyzed by confocal microscopy. Scale bars of panels and zooms from squared area represent 10µm and 2µm, respectively. Colocalized pixels (white channel) between red, green and blue channels were extracted with the ColocalizeRGB plugin of ImageJ. (**B**) The surface and (**C**) the number of core/NS4B/NS5A and NS4B/NS5A structures were quantified with ImageJ. For each condition, 30-50 cells were quantified. ****, P≤0.0001; ***, P≤0.001; **, P≤0.01; *, P≤0.05; ns (not significant), P>0.05.

Supplemental Figure 5. Analysis of phosphorylated forms of NS5A. Huh7.5 cells were infected with Jc1 or Jc1-Y93H viruses at an MOI of 0.2. At 66h post-infection, cells were washed and incubated with 1nM of DCV or DMSO for the indicated time. Infected cells were harvested at 2, 4, 6 or 24h following initiation of DCV-treatment and expression of calnexin (CNX) and NS5A proteins was analyzed by Western Blot. (**A)** A representative experiment is shown. The lower (*) and upper (**) NS5A bands correspond to basal (p56) and hyperphosphorylated (p58) forms of NS5A, respectively. The intensity of each band was quantified by densitometry with ImageJ. The ratio of p58/total NS5A normalized to the internal control calnexin (CNX) (designated % p58) is indicated below each lane. The values determined for mock-treated samples at each timepoint were set to 100%. (**B**) The means of the ratio of p58/total NS5A following DCV treatment from 3 independent experiments are shown.

Supplemental Figure 6. Analysis of subcellular distribution of HCV proteins in Jc1-infected cells upon DCV treatment. (A) Huh7.5 cells transfected with Jc1 full-length genome RNA were incubated with 1nM of DCV or DMSO at 66h post-transfection. Transfected cells were lysed at 6h following initiation of DCV-treatment and were fractionated on iodixanol gradients. Each fraction was analyzed by Western blotting using antibodies against calnexin (CNX), HCV NS5A, E2, core and NS4B proteins, and Adipose differentiation-related protein (ADRP). 1/50 of unfractionated post-nuclear extracts (PNE) were also analyzed. Results are representative of 5 independent experiments. (**B**) Huh7.5 cells were infected with Jc1 (lefts panels) or Jc1-Y93H (right panel) viruses at an MOI of 0.2. At 66h post-infection, infected cells were washed and incubated with 1nM of DCV or DMSO. After 6h of DCV treatment, cells were fixed and then stained for HCV core, NS5A and NS4B proteins and for lipid droplets (LDs). Colocalization of core and NS4B or core and NS5A proteins with LDs was analyzed by confocal microscopy. The percentage of core/NS4B (left panel) or core/NS5A punctate structures apposed at the edges of LDs in Jc1 (middle panel) or Jc1-Y93H (right panel) infected cells were quantified with ImageJ. ns (not significant), P>0.05.

Supplemental Figure 7. Structural proteins and NS4B colocalize within discrete structures. Huh7.5 cells were infected with Jc1 at an MOI of 0.2 and were fixed at the indicated times post-infection. Cells were then stained for HCV E2, core and NS4B proteins and the colocalization of core proteins with E2 and NS4B was analyzed by confocal microscopy. The merge of the three channels, as well as individual channels for E2, core and NS4B proteins (green, red and white channel respectively) are represented. Scale bars of panels and zooms from squared area represent 10µm and 2µm, respectively.

Supplemental Figure 8. Kinetics of HCV core distribution within infected cells. Huh7.5 cells were infected with JFH1 or Jc1 viruses at an MOI of 0.2 and cultured for the indicated timepoints with or without a 24h-treatment with 20µg/mL of cycloheximide (CHX) from 24h or from 48h post-infection, as indicated. Cells were fixed at 16h, 24h, 48h or 72h post-infection, as indicated, and then stained for HCV core and lipid droplets (LDs). (**A**) Colocalization of core protein (red channel) with LDs (green channel) was analyzed by confocal microscopy. Scale bars of panels and zooms from squared area represent 10µm and 2µm, respectively. (**B**) The size and (**C**) the number of core punctate structures in CHX treated cells were quantified with ImageJ. For each condition, 30-50 cells were quantified. ****, P≤0.0001; ***, P≤0.001; **, P≤0.01; *, P≤0.05; ns (not significant), P>0.05; ND, not determined.

Supplemental Figure 9. DGAT1 down-regulation or inhibition induce the clustering of E2/core/NS4B and E2/core/NS5A structures. Huh7.5 cells were transduced with pLKO.1-puro empty vector (Ctrl) or with pLKO.1-puro vector with DGAT1 shRNA (shDGAT1). Seven days post-transduction, down-regulated cells were infected with Jc1 virus at an MOI of 0.2. In separate experiments, Huh7.5 cells were infected with Jc1 virus at an MOI of 0.2 and treated with 150µM of the DGAT1 inhibitor A922500 or DMSO. In both conditions, cells were fixed at 72H post-infection, stained for HCV E2, core and NS4B or NS5A proteins and the colocalization of core protein with E2 and NS4B or with E2 and NS5A was analyzed by confocal microscopy. (**A**) The expression of DGAT1 and calnexin (CNX) and core proteins at 72h post-infection was analyzed by Western blot. (**B**) The intracellular or extracellular infectivity were determined from cell lysates or supernatants of infected cells, respectively. (**C**) The surface (left panel) and the number (right panel) of E2/core/NS4B and E2/core/NS5A structures were quantified with ImageJ. (**D**) The intracellular or extracellular infectivity were determined from cell lysates or supernatants of infected cells, respectively. (**E**) The surface (left panel) and the number (right panel) of E2/core/NS4B and E2/core/NS5A structures were quantified with ImageJ. For each condition, 20 cells were quantified. ****, P≤0.0001; ***, P≤0.001; **, P≤0.01; *, P≤0.05; ns (not significant), P>0.05.